

出國報告(出國類別:研習會)

南海內潮及內波之研究

服務機關：海軍軍官學校

姓名職稱：楊穎堅

派赴國家：奧地利

報告日期：100 年 5 月 12 日

2 出國時間：100 年 3 月 31 日—100 年 4 月 9 日

目錄

目錄.....	1
摘要.....	2
目的.....	3
會議過程.....	3
會議心得與收穫.....	3
建議事項.....	4
附錄一：發表論文.....	5
附錄二：與會照片.....	16

摘要

於 100年 3月 31日至 4月 9日期間，前往奧地利維也納市參加歐洲地球科學聯盟 (European Geosciences Union)舉辦之 2011年聯合會(General Assembly 2011)，吸收最新之地球科學研究成果，並發表國科會專題研究計畫之內波研究成果，論文名稱為：Pressure perturbations induced by mode-1 depression internal solitary waves。

Yiing Jang Yang (1), Ren-Chieh Lien (2), Ming-Huei Chang (3), and Tswen Yung Tang (4) (1) Naval Academy, Kaohsiung, Taiwan (yjyang@cna.edu.tw), (2) Oceanographic Laboratory, University of Science and Technology of China, Hefei, China, (3) Department of Marine Environmental Science, National Sun Yat-sen University, Keelung, Taiwan, (4) Department of Oceanography, National Taiwan University, Taipei, Taiwan

Large-amplitude mode-1 depression internal solitary waves produce pressure perturbations of $O(10\text{ cm})$ near the bottom in the South China Sea. Comparing with ADCP measurements near the bottom, the observed pressure perturbation is predicted well by the Bernoulli balance. The difference is likely due to effects of the diabatic process and that the streamline is not at constant depth near the bottom. The nonhydrostatic component of pressure perturbations has an opposite sign at the trough and the same sign at the front and rear ends of solitary internal waves. The shape of observed pressure perturbations is perfectly correlated with that predicted from the Bernoulli balance. This analysis concludes that internal solitary waves can be captured directly from a bottom mounted pressure sensor. Providing the wave speed and stratification profile, the kinematic properties of internal solitary waves could be inferred from pressure perturbations at the bottom.

出席國際會議心得報告

1 目的：

與國際著名學者討論南海內潮及內波並發表個人論文。

2 會議過程：

由於國籍航空(長榮與華航)往返奧地利維也納市的班機並非日有，而是每兩天方有班機往返。故主持人選擇長榮班機於 2011 年 4 月 1 日早上到達奧地利維也納市、於 2011 年 4 月 8 日傍晚會議結束後立即搭機返國。參與會議經過，如下所述：

主持人於 2011 年 3 月 31 日晚上由桃園國際機場出關前往奧地利維也納市，於隔日(4 月 1 日)上午到達目的地旅社後即稍作休息。3~8 日參加研討會，並於 4 月 6 日上午發表論文，論文題目為 Pressure perturbations induced by mode-1 depression internal solitary waves，內容主要敘述在南海北部陸棚邊緣的第一斜壓模態內孤立波所引發的海底壓力變化，並藉由白努力關係式探討海床壓力與水層流速之關聯、以及第一斜壓模態內孤立波所引發之非靜水壓力變化。

會議期間，主持人亦曾與一些國際著名之內波研究學者一起討論南海的非線性內波及我的論文研究成果，以及討論未來共同合作研究的可行性。

研討會於 4 月 8 日傍晚結束，主持人隨即前往機場搭機返國，於 4 月 9 日傍晚返抵國門。

3 會議心得與收穫：

會議期間，主持人亦曾與一些相關的研究人員進行討論，例如：

3.1 在發表論文” Pressure perturbations induced by mode-1 depression internal solitary waves” 期間，有數位學者針對此論文內容討論熱烈，收穫良多。期間有些學者建議將其發表於 SCI 期刊。主持人返國後，即與其他共同作者討論，並彙整議場意見，撰寫成正式論文，目前已近乎完成初稿，預定於短期內投稿。

3.2 來自德國 Institut für Umwelphysik, Universität Bremen 之 Dr. Uwe Stöber 所發表的論文為” Automated detection of nonlinear internal waves from seafloor pressure time series”，其內容主要是利用海床壓力計的即時資料來偵測內波。此論文的資料與研究內容與我們的論文近似，故主持人與 Dr. Uwe Stöber 有深入的討論其研究細節與成果。

3.3 來自英國 School of Marine Science and Engineering, University of Plymouth,

Plymouth之博士生Mr. Chuncheng Guo所發表的論文為” Numerical simulation on the transformation of large amplitude second mode internal solitary waves over a slope-shelf topography” ，其內容主要是參考主持人先前所發表的兩篇論文進行更深入的探討，Mr. Guo 與我是第一次見面，他非常高興能與參考論文的作者會面並討論。

- 3.4 來自俄羅斯 Institute of Applied Physics, Nizhny Novgorod 之 Dr. Ekaterina Ruvinskaya 所發表的論文為” Nonlinear dynamics of intensive internal waves in bounded stratified basins” ，其內容主要是內波的理論計算。由於俄羅斯的學者對於內波的研究主要是專注於理論部分，較缺乏現場的觀測資料。故 Dr. Ekaterina Ruvinskaya 希望提供一些已發表之關於內波觀測的論文供其參考，並期望未來能有合作的機會。
- 3.5 會議期間，主持人亦聆聽到國際知名內波研究學者 Dr. Roger Grimshaw 與 Dr. Tatiana Talipova 的專題報告，題目分別為” The effect of rotation on internal solitary waves” 、” Modulation instability and hazardous internal waves in South China and Baltic Seas” ，收穫良多。
- 3.6 會議期間，原預定與來自俄羅斯 Andreyev Acoustics Institute, Moscow 的國際知名的內波研究學者 Dr. Andrey Serebryany 一起討論南海的內波。其來信告知臨時來信無法與會，於是我們乃借由 email 討論。他將於今年 11 月拜訪台灣，屆時我們將召開一個臺俄內波學術研討會，與國內的內波研究人員共同討論。

4 建議事項：

此次讓個人受益良多，建議可多鼓勵國內學者至國外研習。

附錄一：論文

1. Introduction

In the northern SCS, NLIWs have often been observed in satellite images (Hsu and Liu, 2000; Zhao et al., 2004), in-situ measurements (Alford et al., 2010; Ramp et al., 2006; Yang et al., 2006; Chang et al., 2006; Lien et al., 2005) (Fig. 1). These waves propagate westward across deep basin as KdV wave without significant change of their characteristics (Klymak et al 2006). To the east of Dongsha plateau, these wave encounter shoaling Dongsha slope, reduce propagation speed (Alford et al 2010), develop trapped core and wave trains (Lien 2010). Across the Dongsha plateau, NLIW loses most of its energy (Chang et al 2006).

Reader and Ma (personal communication) observed distinct sand ripples and elevated bottom sediment concentration after the passage of NLIWs. It has been speculated that NLIWs may trigger sediment resuspension. Pressure perturbation and vortex ejection between sand ripples are possible mechanism for disturb and lift sediments. Moum and Smyth (2006) computed non-hydrostatic pressure, $25\text{-}90\text{ N m}^{-2}$ ($\sim 0.25\text{-}0.9\text{ cm}$), external hydrostatic pressure, $-(1\text{-}90)\text{ Nm}^{-2}$, and the internal hydrostatic pressure, $100\text{-}300\text{ N m}^{-2}$, caused by elevation waves of $12\text{-}33\text{-m}$ amplitude on the continental slope. The net pressure perturbation was positive for elevation waves. They inferred that depression NLIWs should cause negative pressure perturbation. Moum and Nash (2007) later confirmed negative pressure perturbation $200\text{-}300\text{ N m}^{-2}$ caused by depression NLIWs, again dominated by internal hydrostatic pressure. In both cases, they found the pressure perturbation proportional to the wave amplitude.

It is generally believed that vortex ejection might be an efficient mechanism for sediment resuspension than pressure perturbation (Diamesis and Redekopp, 2006; Diamesis and Redekopp, 2010). In the case of large pressure perturbation, caused by large-amplitude NLIWs in South China Sea, its effect for sediment resuspension might become more important. In this analysis, we present pressure perturbation as large as 4000 Nm^{-2} , i.e, about 1.5 order of magnitude greater than that observed by Moum and Smyth (2006) and Moum and Nash (2007), caused by $O(100\text{-m})$ -amplitude NLIWs.

The experiment and instruments are described in Section 2. In Section 3, we present pressure observations and the extraction of high-frequency pressure perturbations associated with solitary internal waves. In Section 4, we review Bernoulli equations. In Section 5, we compute the pressure perturbation using Bernoulli balance, and the non-hydrostatic component of pressure perturbations. These estimates are compared with observed pressure perturbation. In Section 6, we present results of fully nonlinear internal waves predicted using DJL. We discuss inferences of bottom pressure perturbations and summarize analysis results in Section 7.

2. Experiment and Solitary Internal Waves

Four bottom mounted moorings were deployed between June 2006 and May 2007 in the northern South China Sea to study nonlinear internal waves (Fig. 1). On each mooring, an upward-looking 75-kHz ADCP was housed in a syntactic-foam float at 10 m above the bottom (mab). The ADCP had a blanking length of 8 m, and a vertical bin size of 16 m. Therefore, the deepest velocity measurement centered at 26 mab. The ADCP pinged every 90 s, and took reliable velocity measurements from 26 mab to about 50 m below the sea surface. The near surface velocity measurements were contaminated by sea

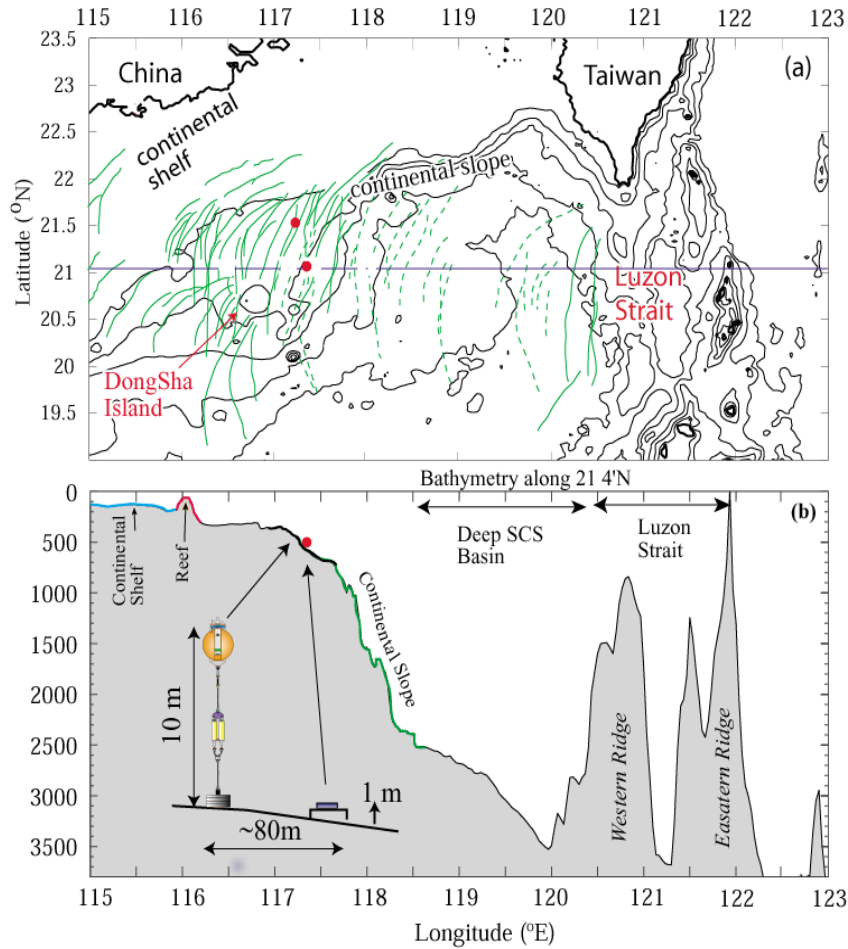


Fig. 1: (a) Bathymetry map in South China Sea and a composite view of the appearance of solitary internal waves on satellite images (Zhao et al 2004), solid green curves for wave trains and dashed green curves for single depression wave, (b) bathymetry along $21^{\circ} 05' N$. Red dots indicate locations of measurements of pressure sensor and bottom mounted ADCP. Note that the ADCP mooring and the pressure mooring are separated by ~ 80 m. The ADCP mooring was located at 586-m depth and the pressure mooring at 613-m depth. The deepest ADCP measurements are at 550-m depth and the pressure sensor is at 612-m, 1 m off the bottom.

Two bottom pressure moorings were deployed between April 13 and May 7 2007 within a close range, ~ 80 m, from two ADCP moorings (red dots in Fig. 1a). The pressure sensor was mounted on a frame which is attached to the anchor. The pressure sensor depth was at 1 mab and took measurements every 60 s (Fig. 1b). The accuracy of the pressure sensor is ~ 0.5 cm, estimated from spectral white noise floor, sufficient for measuring the pressure perturbation, $O(10$ s cm), caused by large-amplitude NLIWs in SCS. We focus our analysis on the southern pressure data at $117^{\circ} 21' E$ $21^{\circ} 05' N$, 586-m water depth, where the NLIWs are much larger and the NLIW properties are better determined. This mooring site was called LR1 in Alford et al (2010) and Lien et al (2010). Lien (2010) showed that the property of NLIW at LR1 was well predicted by fully-nonlinear, steady, and non-dissipative Dubriel-Jacotin-Long (DJL) model. When NLIWs propagated further up the slope, they responded strongly to the bottom, may

developed trapped core, and became turbulent. Therefore, DJL solution might not be suitable for predicting NLIWs further west of LR1. Later, we will compare pressure perturbation predicted by DJL with observations.

3. Pressure Perturbations and Signals of Solitary Internal Waves

Pressure observations at 1 mab show apparent spring and neap cycle, with ~ 1.2 -m peak-trough amplitude in the spring tide and ~ 0.2 -m in the neap tide (Fig. 2). Both diurnal and semidiurnal tides are present, with stronger diurnal component. These are mostly local barotropic tidal signal. High-frequency pressure perturbations associated with solitary internal waves appear mostly during the spring tide, nearly semidiurnally. The appearance of high-frequency pressure perturbation does not seem to be locked in phase with low-frequency pressure perturbation. It is generally believed that the solitary internal waves in SCS is either generated via or somehow related to internal tides in Luzon Strait where semidiurnal tide is as strong as the diurnal tide. Therefore it is not unexpected that the solitary internal wave (high-frequency pressure perturbations) at LR1 is not phase locked with the local barotropic tide (low-frequency pressure perturbations).

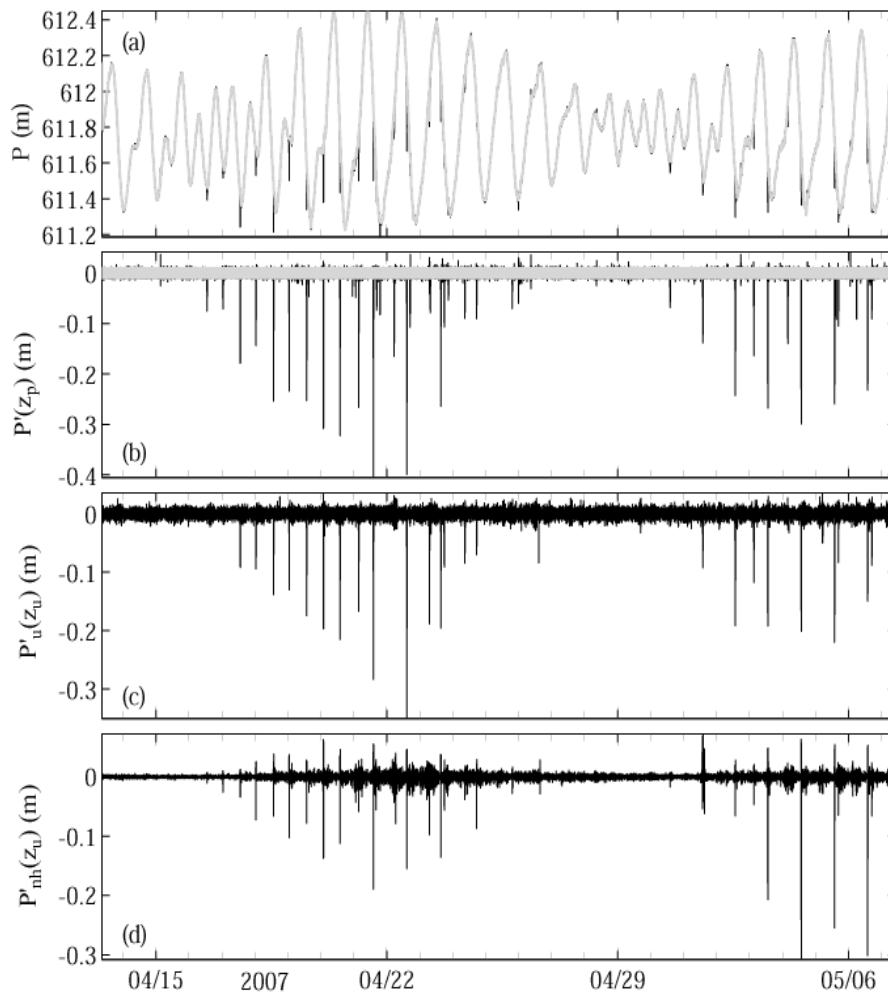


Figure 2: Time series of (a) pressure perturbations at 1 mab, (b) pressure perturbations due to solitary internal waves (see Fig. 3 for its derivation), (3) pressure perturbations estimated using the Bernoulli balance and moored ADCP velocity measurements, and (4) the non-hydrostatic component of pressure perturbations estimated from moored ADCP profiles. In panel (a), the black curve is the observed pressure perturbation, and the grey curve is the low-passed of the observed pressure after removing the high-frequency signal, explained in Fig. 3.

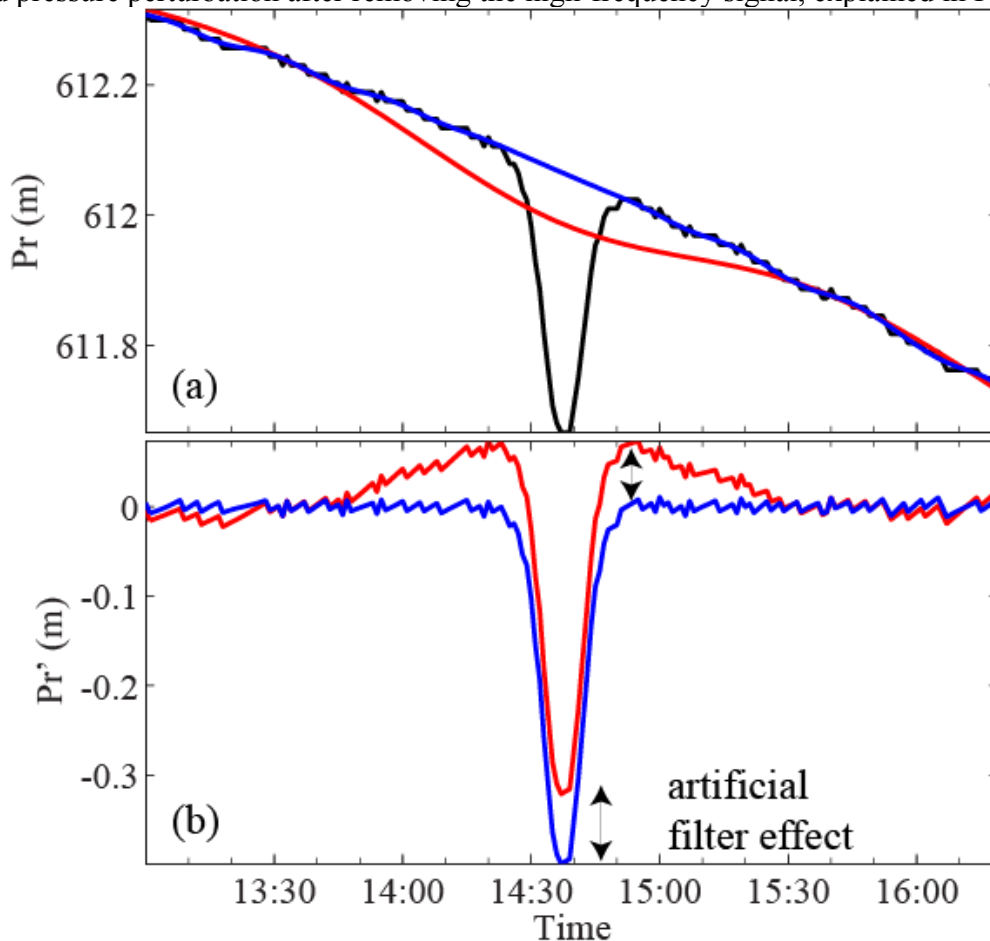


Figure 3: Illustration of extracting pressure perturbation associated with solitary internal waves. Panel (a) shows the observed pressure (black curve) including one high-frequency solitary wave event, the red curve is 1-hr low-pass filtered pressure, and the blue curve is the 1-hr low-pass filtered pressure after first removing the high-frequency signal. Panel (b) shows two different estimates of high-frequency perturbation. The red curve (wrong estimate) is the pressure perturbation computed by removing the straight low-pass filtered pressure (red curve in a) from the observations (black curve in a), and the blue curve (correct estimate) is computed by removing the low-pass filtered pressure without the high-frequency internal waves (blue curve in a) from the observations (black curve in a). The lines with double arrowhead indicate the artificial filter effect by reducing the high-frequency pressure signal at the center of the wave and adding artificial pressure perturbations at the front and rear ends of the wave.

Extracting high-frequency pressure perturbation signals from observations is nontrivial. We found that using a high-pass filter degrades the high-frequency signal and, even-worse, it introduces biases at the beginning and two ends of high-frequency perturbations (Fig. 3). To appropriately extract the localized high-frequency perturbations and avoid end effects, we (1) identify high-frequency events with pressure perturbations greater than 2 cm, (2) construct a new pressure time series excluding high-frequency events and linearly interpolating the missing pressure segment, (3) low-pass filter the new time series of pressure (blue curve in Fig. 3a). The new time series of low-pass filtered pressure does not contain the effects of high-frequency pressure perturbations. The high-frequency pressure perturbation (Fig. 2b and 3b) is computed as the difference between the original pressure observations (black curve in Fig. 2a) and (3) (grey curve in Fig. 2a).

We have identified 29 NLIW events with the maximum pressure perturbations greater than 4 cm in the 24-day period. All have negative pressure perturbations, ranging from 4 cm to 40 cm, with 14 events greater than 20 cm. Note these pressure perturbations are more than one order of magnitude greater than those observed by Moum and Smyth (2006) and Moum and Nash (2007).

4. Review of Bernoulli Balance

Moum and Smyth (2006) discuss three components of pressure perturbation induced by elevation solitary internal waves, i.e., the surface elevation (external hydrostatic), the non-hydrostatic, and internal hydrostatic component. The internal hydrostatic pressure has the strongest signal. Moum and Nash (2007) discuss the depression solitary internal waves and yield the similar conclusion.

We do not have measurements of density accompanying the pressure observations, and will not discuss the various components of pressure perturbations. Instead, we would like to investigate the Bernoulli balance where the pressure perturbation is balanced with kinetic energy, and isopycnal displacement. Since the isopycnal displacement near the bottom is negligible, the balance is simply between kinetic energy and pressure perturbation (to be shown later). It suggests that the bottom pressure sensor might be a useful parameter for the measure of kinetic energy of NLIWs. We

First, we will review the Bernoulli equation following Kundu (2007). The adiabatic momentum equation can be rewritten as

$$\frac{\partial \underline{u}}{\partial t} + \nabla B = \underline{u} \times \underline{\omega} \quad (1)$$

$$B = \frac{1}{2}(u^2 + v^2 + w^2) + P + gz \quad (2)$$

Here, B is the Bernoulli function, z the vertical coordinate, P the kinematic pressure, \underline{u} the velocity vector, g the gravity, and $\underline{\omega}$ the relative vorticity vector. Assuming that the wave is steady on the reference frame of moving with the wave during the period when passing the mooring site, i.e. typically 10-20 minutes (Fig. 3), 2-dimensional, i.e., $v \equiv 0$, and propagates at a speed of C , Bernoulli equation and function on the wave-moving frame become

$$\nabla B = \underline{u} \times \underline{\omega} \quad (3)$$

$$B = \frac{1}{2}[(u - C)^2 + w^2] + P + gz \quad (4)$$

$$\begin{aligned} u &= \partial_z \psi \\ w &= -\partial_x \psi \end{aligned} \quad (5)$$

Therefore, (3) implies that the Bernoulli function B must be constant along the stream line

$$B(\psi) = \frac{1}{2}[(u(\psi) - C)^2 + w(\psi)^2] + P(\psi) + gz(\psi) = B_0 \quad (6)$$

Note that the streamline is a function of x and z . In the absence of background flow, the Bernoulli function outside of the wave becomes

$$B_0 = \frac{1}{2}C^2 + P_0(\psi) + gz(\psi) \quad (7)$$

The zero-normal flow condition assures that the bottom boundary is a streamline. The pressure sensor is located at z_p , 1 mab. At 1 mab, the vertical displacement of streamline is negligible. In other words, Bernoulli function should be constant at z_p . Bernoulli function and pressure perturbation can be written as

$$B(x, z_p) = \frac{1}{2}[(u(x, z_p) - C)^2 + w(x, z_p)^2] + P(x, z_p) + gz_p = B_0 = \frac{1}{2}C^2 + P(x_0, z_p) + gz_p \quad (8)$$

$$P'(x, z_p) = P(x, z_p) - P(x_0, z_p) = \frac{1}{2}[(u(x, z_p) - C)^2 + w(x, z_p)^2 - C^2] \quad (9)$$

In this analysis, we will compare observed pressure perturbation (the left hand side) with the prediction from the Bernoulli balance $\hat{P}'(x, z_u)$

$$\hat{P}'(x, z_u) = \text{EMBED Equation. 3} \quad (10)$$

where $z_u \sim 26$ mab is the deepest velocity measurements from ADCP. The bottom ADCP measurements are separated from pressure measurements by ~ 80 m horizontally. We will demonstrate that $P'(x, z_p)$ and $\hat{P}'(x, z_u)$ are strongly correlated and discuss the effect of vertical separation. The assumption of flat streamline will be discussed using DJL modeled solitary internal waves.

The wave speed is needed to compute $\hat{P}'(x, z_u)$. The propagation speed of solitary internal waves in this area changes rapidly due to its response to bottom topography. Chang et al (2010) derive a technique to estimate the propagation direction and propagation speed using moored ADCP measurements. The technique is confirmed by comparing estimates with the propagation direction observations from marine radar and with the propagation speed computed from arrival time of waves passing by adjacent moorings. Only near-bottom velocity measurements are used in order to avoid beam spreading effect. Our of 29 pressure perturbation events, 17 estimates of wave speed converge and have standard error less than 0.2 ms^{-1} , about 10% of mean speed. The average wave speed is 2.1 m s^{-1} , ranging from 1.84 to 2.67 ms^{-1} and the prevailing direction is $286 (\pm 8)$ degrees true north, i.e., NWW. We will compute $\hat{P}'(x, z_u)$ of these 17 waves using ADCP velocity measurements closest to the bottom, i.e. 28 mab, and compare with $P'(x, z_p)$ observed at 1 mab.

5. Comparison between Estimated and Observed Pressure Perturbations

Before applying (10), the following procedures are taken. First, we rotate the horizontal coordinate into (x', y') , where x' is along the propagation direction of wave, and y' perpendicular to the propagation direction. Therefore, u' and v' is velocity component in the propagation direction wave and the velocity component perpendicular to the wave's propagation direction, respectively. In the following analysis, we will drop the prime for convenience. Secondly, we remove the background flow

In order to Following (7), we compute $P(z_u)$ ignoring the vertical displacement of stream (Fig.3c). Including the effect of vertical velocity makes no significant changes. Between April 25 and May 7, solitary internal waves are observed during the in-situ observational experiment. The wave speed and direction is determined from the shipboard radar measurements. During this period, the wave propagates predominantly at 295° at a speed about 1.4 m s^{-1} . Velocity measurements are rotated to the wave direction and a constant wave speed is used for the computation.

Other methods for computing the wave speed: assuming the steady state and two dimensional, the wave speed can be computed as

$$C = -\frac{\partial_t u}{\partial_z w}$$

The estimate of C is found by averaging the individual wave event (Fig. 4 contour of C).

$P(z_u)$ fluctuates in unison with $P(z_p)$ with a similar magnitude (Fig. 3b and 3c). A closer look shows that $P(z_p)$ leads $P(z_u)$ by about 0.8 min, corresponding to a horizontal separation of $\sim 67 \text{ m}$. These two pressure perturbations are strongly correlated (Fig. 5).

The temporal structure, or spatial structure assuming a constant wave speed, of pressure perturbations of all events, is shown in Fig. 6. $P(z_u)$ has a similar spatial structure as $P(z_p)$, but the magnitude is only 0.7 of $P(z_p)$. The difference is primarily due to the vertical displacement of streamline and the vertical structure of pressure perturbation.

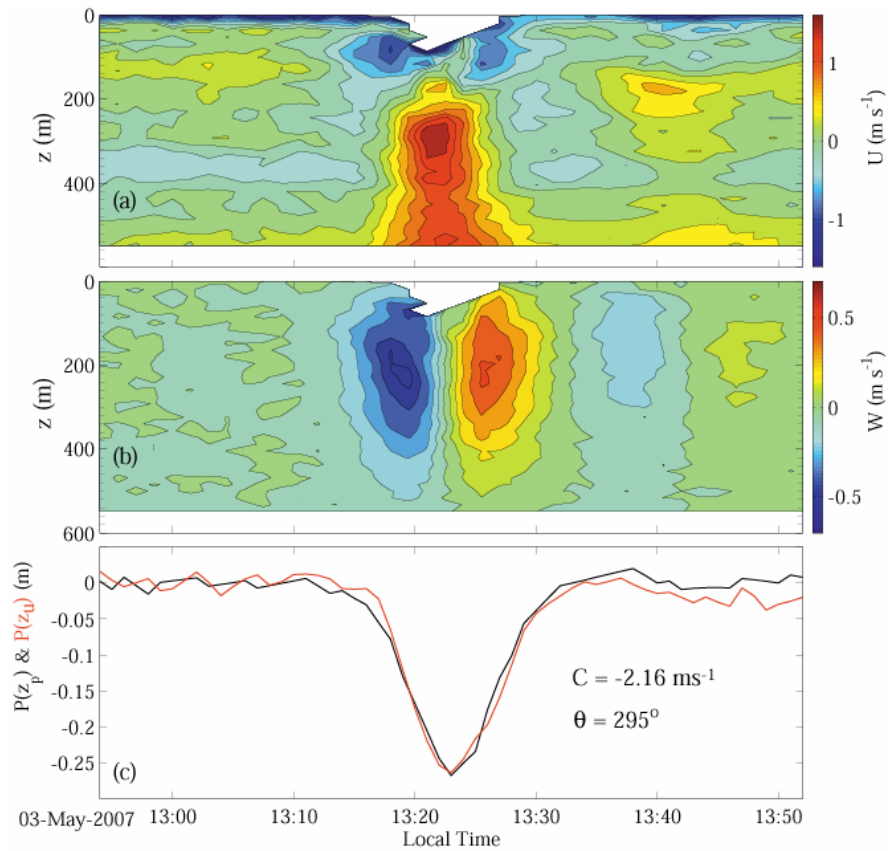


Fig. 3: Example of velocity and pressure perturbations of one solitary internal wave observed at May 2, 2007. The panels (a) and (b) represent the contour of horizontal velocity in the wave propagation direction, and the contour of vertical velocity observed from the bottom mounted ADCP. The panel (c) shows pressure perturbation measured from the near-bottom high-precision pressure sensor (black curve), and the pressure perturbation estimated using the deepest ADCP measurements assuming the Bernoulli balance (red curve), assuming a wave speed of 2.16 ms^{-1} propagating toward 295° true north.

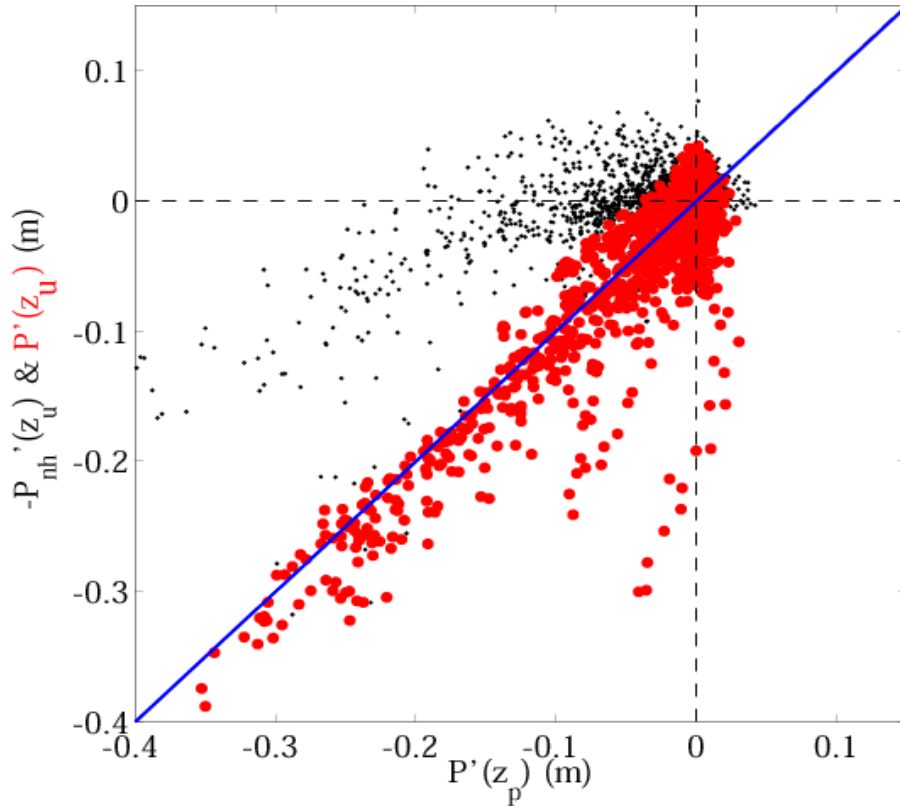


Fig. 5: Comparison between $P(z_u)$ and $P(z_p)$ (red dots), and between $P_{nh}(z_u)$ and $P(z_p)$ (black dots).

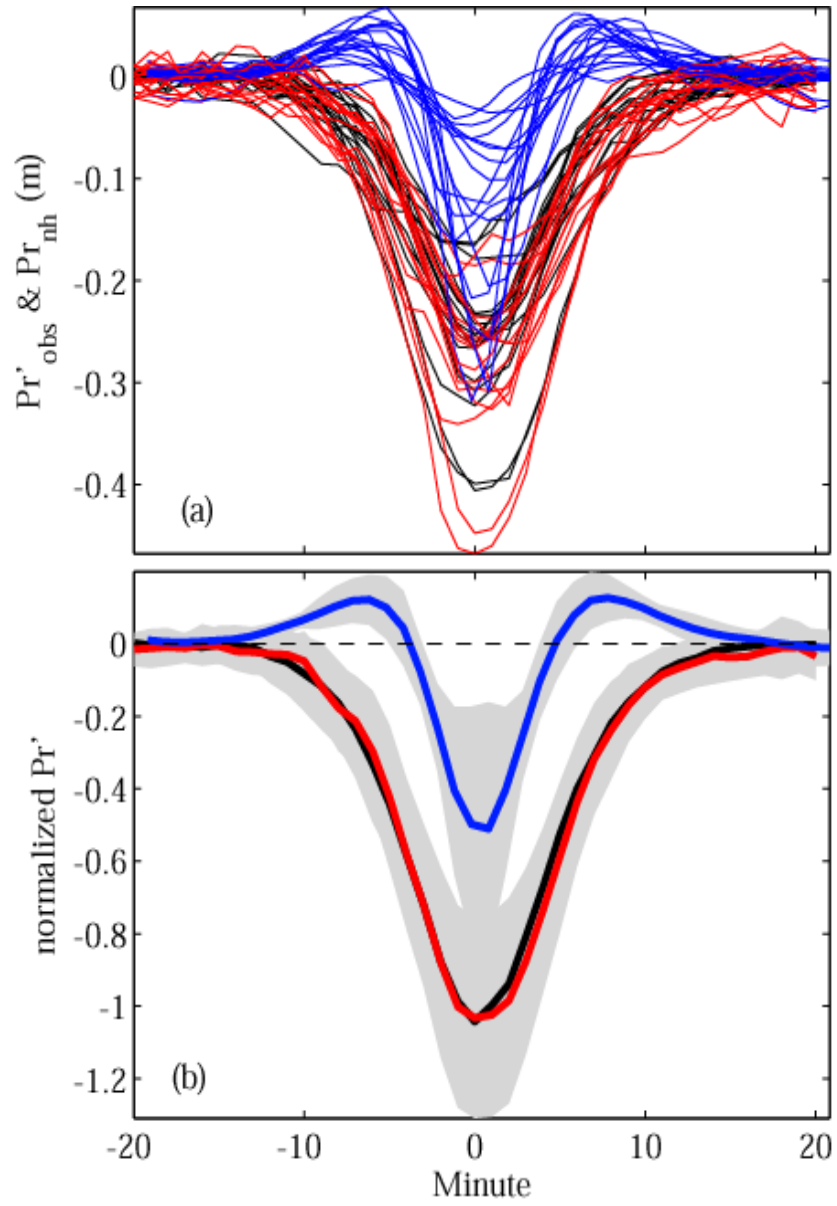
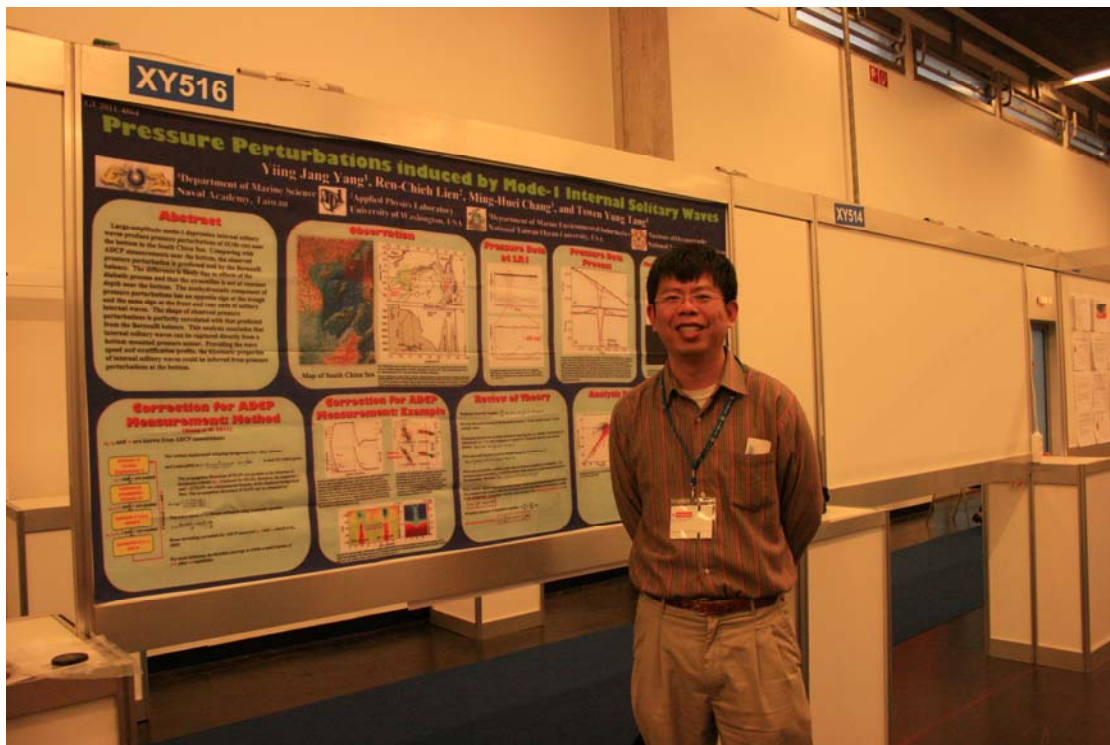


Fig.6: (a) Temporal structure of $P(z_u)$ (red), $P(z_p)$ (black), and $P_{\text{nh}}(z_u)$ (blue), and (b) their normalized form scaled by the top 1/10 of peak $P(z_p)$ of individual event. The shadings indicate one standard deviation. The dashed red curve is $1.4 P(z_u)$, which is nearly identical to $P(z_p)$.

附錄二：與會照片



主持人攝於研討會會場入口



主持人攝於論文海報張貼處